

Supporting Information

Optimally controlled NMR in electrochemistry: Larmor and nutation frequency selective spin excitation for locally selective NMR experiments

Johannes F. Kochs^{1,2,*}, Armin J. Römer^{1,2,*}, Michael Schatz¹, Matthias Streun³, Sven Jovanovic¹, Rüdiger-A. Eichel^{1,4,5}, Simone S. Köcher^{1,6}, and Josef Granwehr^{1,2}

¹Forschungszentrum Jülich GmbH, Institute of Energy Technologies, Fundamental Electrochemistry (IET-1), Jülich, Germany

²Institute of Technical and Macromolecular Chemistry, RWTH Aachen University, Aachen, Germany

³Forschungszentrum Jülich GmbH, Institute of Technology and Engineering (ITE), Jülich, Germany

⁴Institute of Physical Chemistry, RWTH Aachen University, Aachen, Germany

⁵Faculty of Mechanical Engineering, RWTH Aachen University, Aachen, Germany

⁶Fritz Haber Institute of the Max Planck Society, Berlin, Germany

Correspondence: Simone S. Köcher (s.koecher@fz-juelich.de)

Contents

| | | |
|-----------|---|-----------|
| 1 | Pulse shapes of QOC pulses | 2 |
| 1.1 | Larmor-frequency selective pulses | 2 |
| 1.2 | B_1 -selective pulses | 5 |
| 5 | 2 Excitation Profiles | 11 |
| 2.1 | Larmor-frequency selective pulses | 11 |
| 2.2 | Nutation-frequency selective pulses | 13 |
| 3 | Experimental Setup | 16 |
| 3.1 | Setup in FEM simulation | 16 |
| 10 | 4 Supporting measurements | 17 |
| 4.1 | Nutation experiments | 17 |
| 4.2 | B_1 -selective QOC pulse performance | 18 |
| 4.3 | B_0 -selective QOC pulses | 23 |
| 5 | Supporting data | 24 |
| 15 | 5.1 Individual relative integrals of the B_0-selective QOC pulses | 24 |

1 Pulse shapes of QOC pulses

1.1 Larmor-frequency selective pulses

1.1.1 B_1 -robust selective excitation within ± 500 Hz in a ± 2000 Hz suppression band

Figure S1 shows amplitude and phase of the pulse used for B_1 -robust, selective excitation within ± 500 Hz in a ± 2000 Hz suppression band presented in Sec. 3.1 (Fig. 3) of the main article.

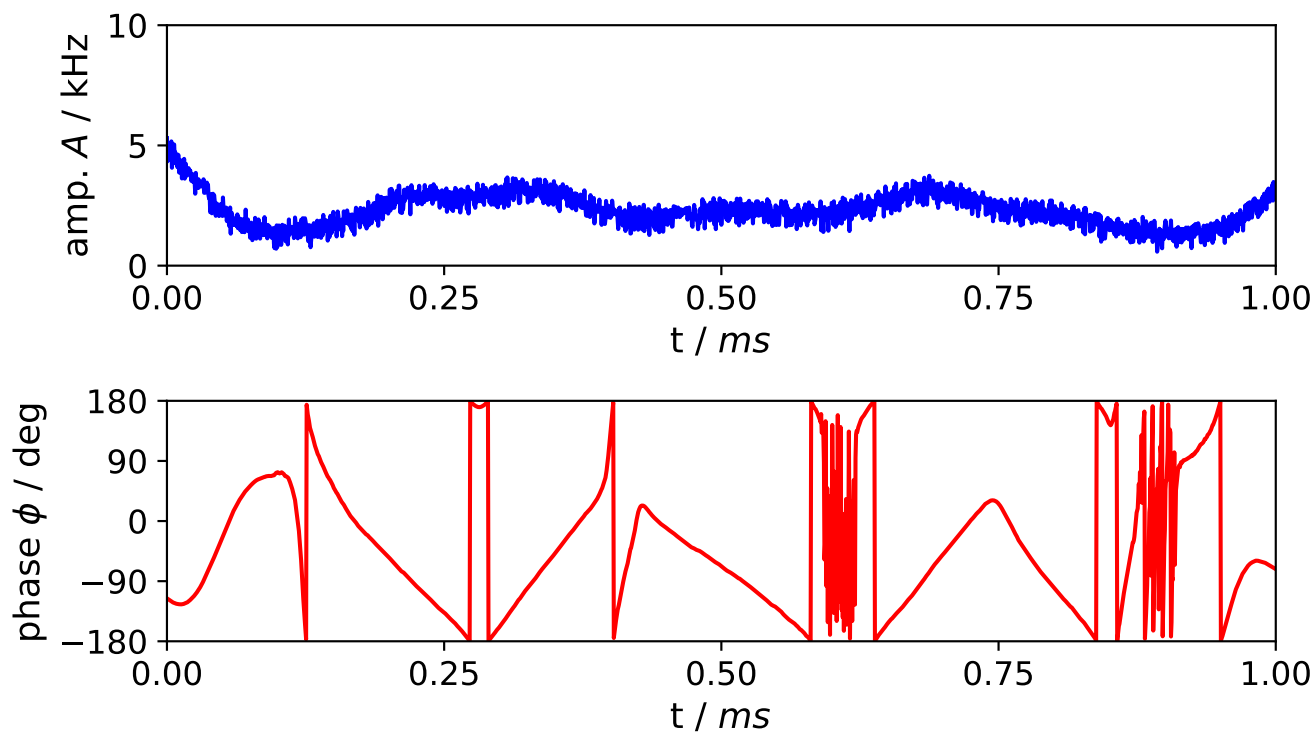


Figure S1. Pulse amplitude A and phase ϕ of the 1 ms Larmor-frequency selective excitation pulse.

1.1.2 B_1 -robust selective suppression within ± 500 Hz in a ± 2000 Hz excitation band

Figure S2 and S3 below show amplitude and phase of the pulses used for B_1 -robust, selective suppression within ± 500 Hz in a ± 2000 Hz excitation band presented in Sec. 3.1 of the main article. The experimental results in Sec. 3.1, Fig. 4 were obtained with the pulse in Fig. S3.

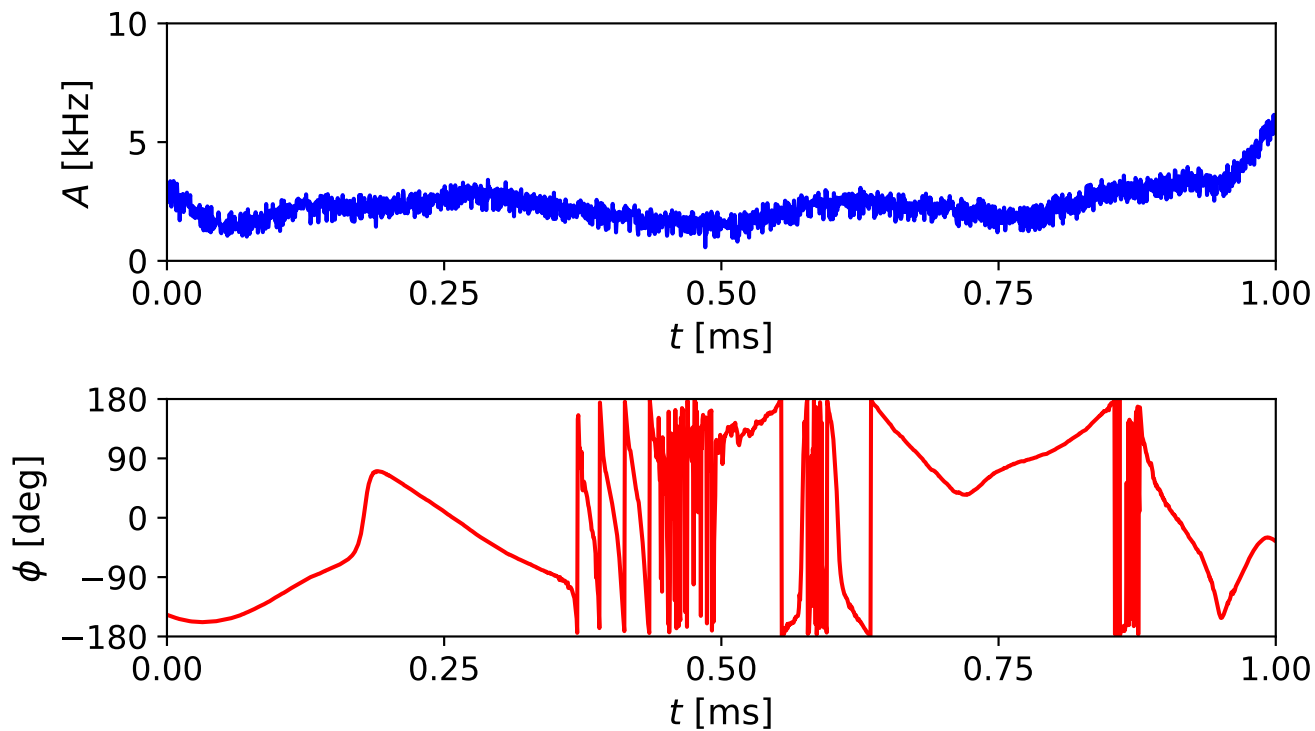


Figure S2. Pulse amplitude A and phase ϕ of the 1 ms Larmor-frequency selective suppression pulse.

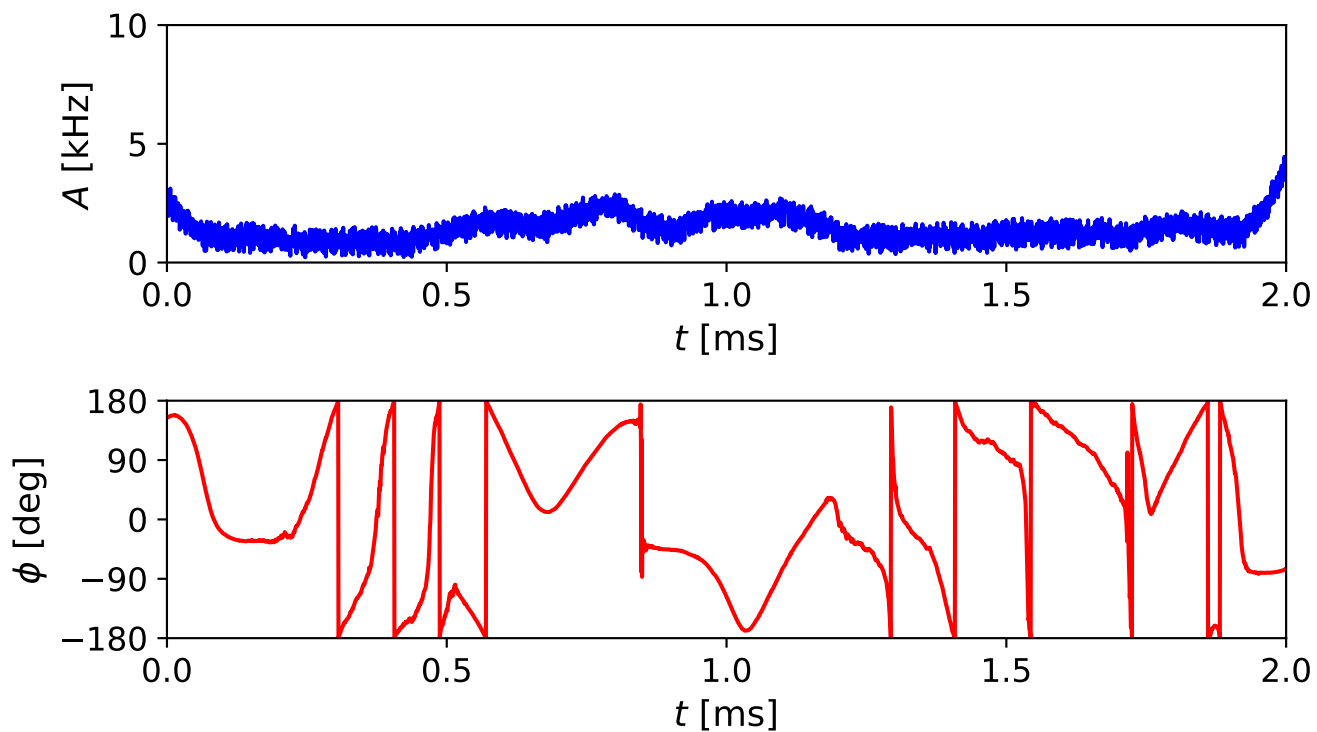


Figure S3. Pulse amplitude A and phase ϕ of the 2 ms Larmor-frequency selective suppression pulse.

The following Figures S4 to S9 show amplitude and phase of the pulses used for Larmor frequency-robust, B_1 -selective excitation for various artificial nutation frequency increases presented in Sec. 3.2 (Fig. 6) of the main article.

1.2.1 Larmor frequency-robust selective excitation for 0 % artificial nutation frequency increase

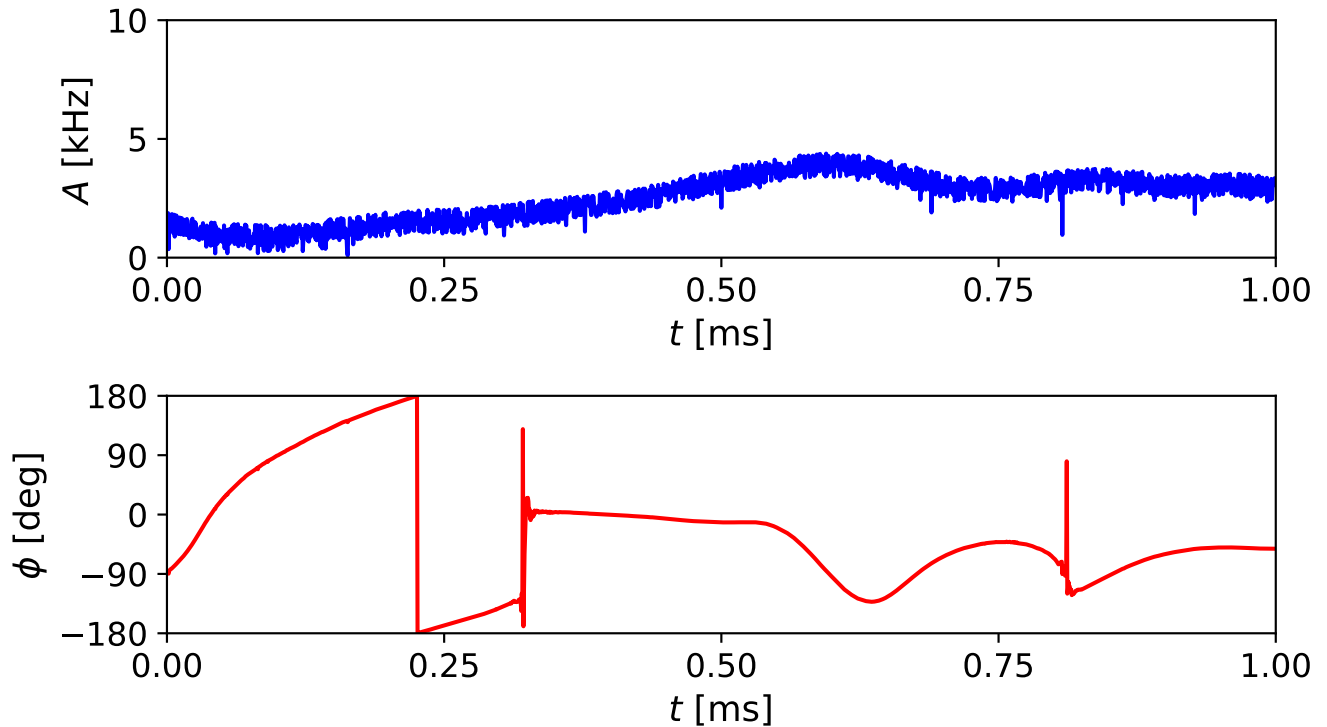


Figure S4. Pulse amplitude A and phase ϕ of nutation-frequency selective excitation for no B_1 increase.

1.2.2 Larmor frequency-robust selective excitation for 20 % artificial nutation frequency increase

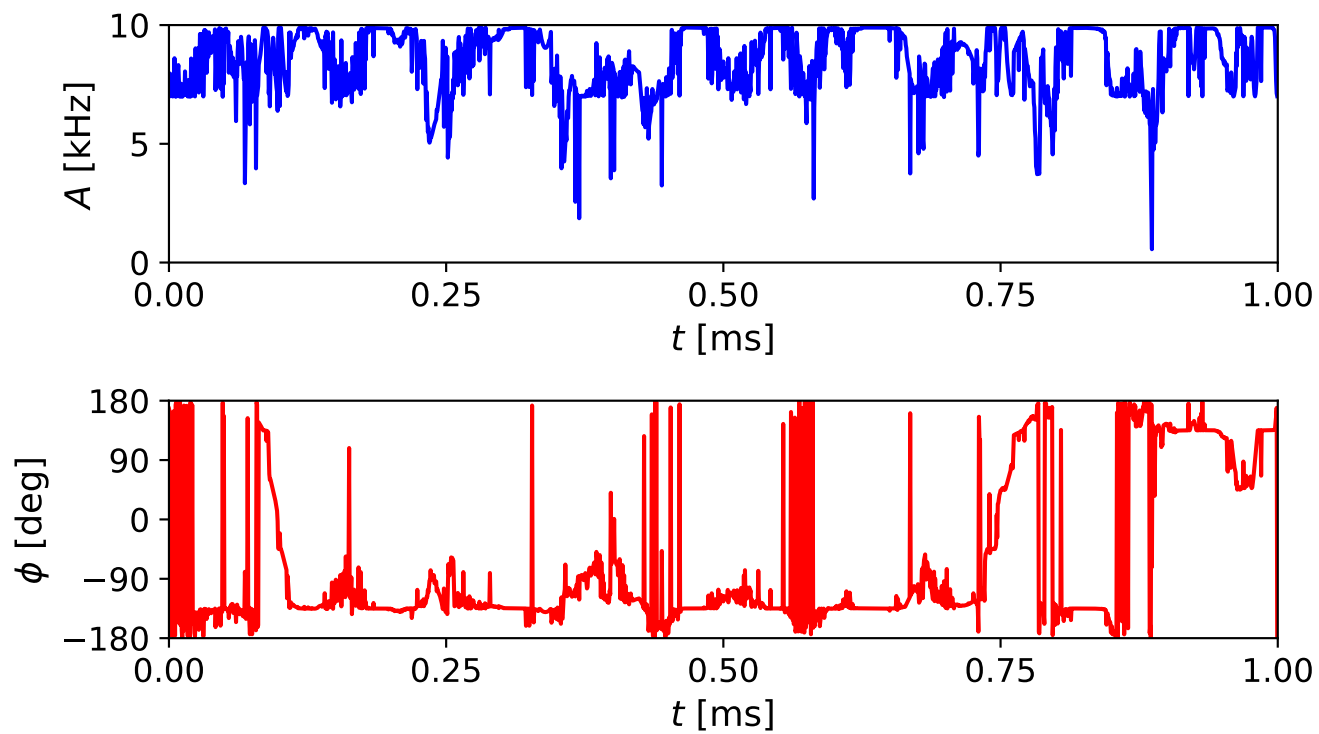


Figure S5. Pulse amplitude A and phase ϕ of nutation-frequency selective excitation for 20 % B_1 increase.

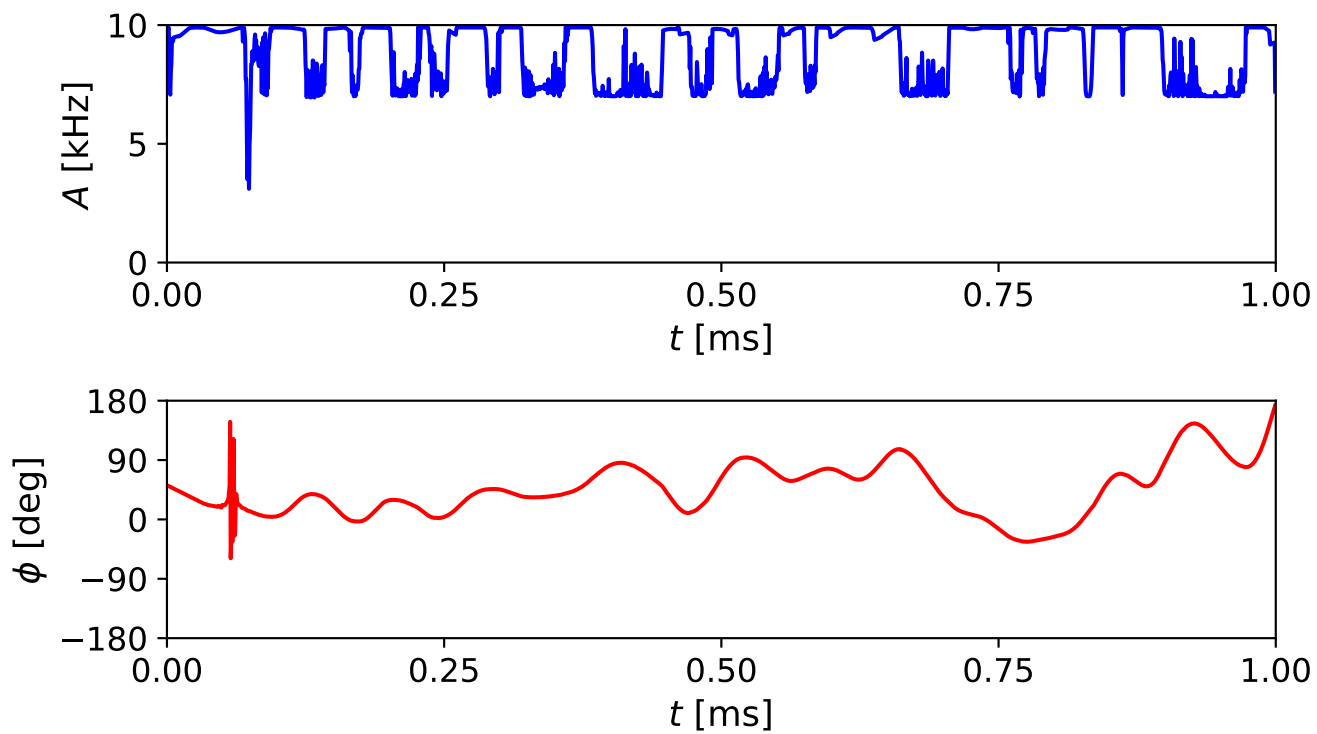


Figure S6. Pulse amplitude A and phase ϕ of nutation-frequency selective excitation for 25 % B_1 increase.

1.2.4 Larmor frequency-robust selective excitation for 30 % artificial nutation frequency increase

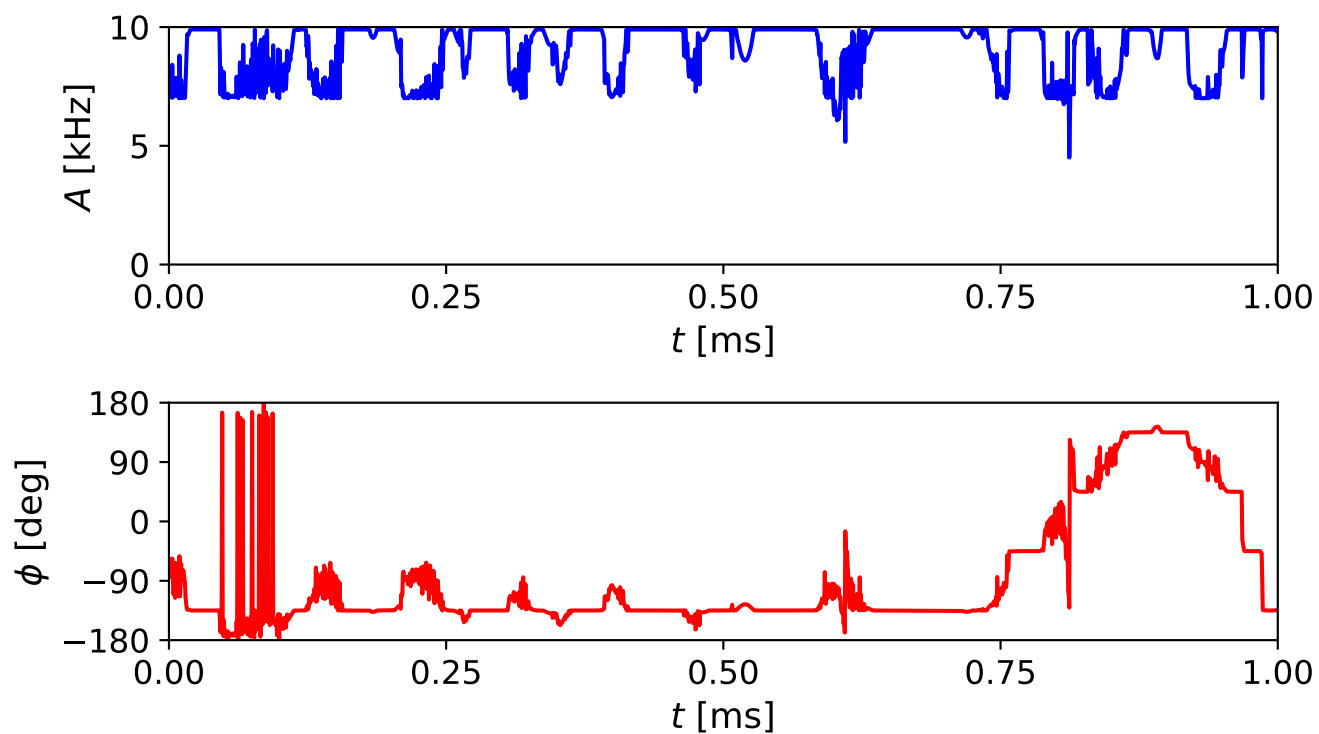


Figure S7. Pulse amplitude A and phase ϕ of nutation-frequency selective excitation for 30 % B_1 increase.

1.2.5 Larmor frequency-robust selective excitation for 40 % artificial nutation frequency increase

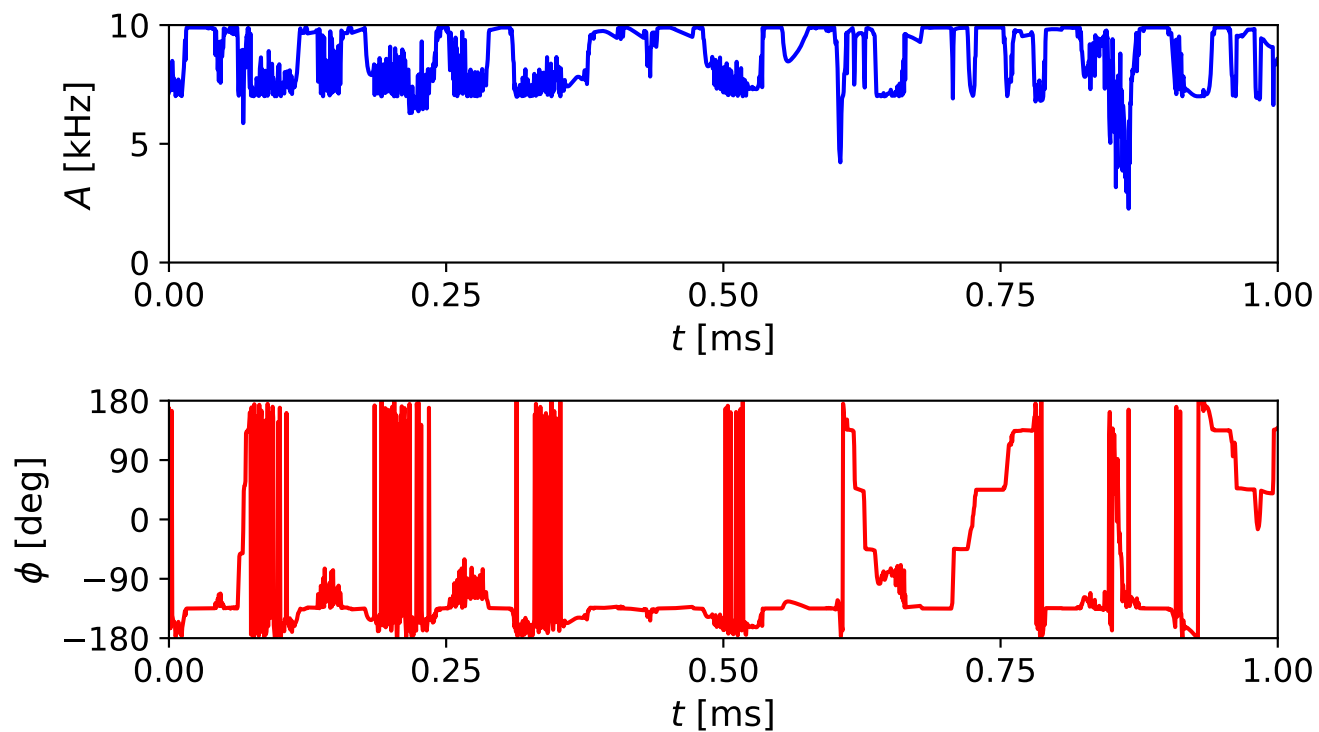


Figure S8. Pulse amplitude A and phase ϕ of nutation-frequency selective excitation for 40 % B_1 increase.

1.2.6 Larmor frequency-robust selective excitation for 80 % artificial nutation frequency increase

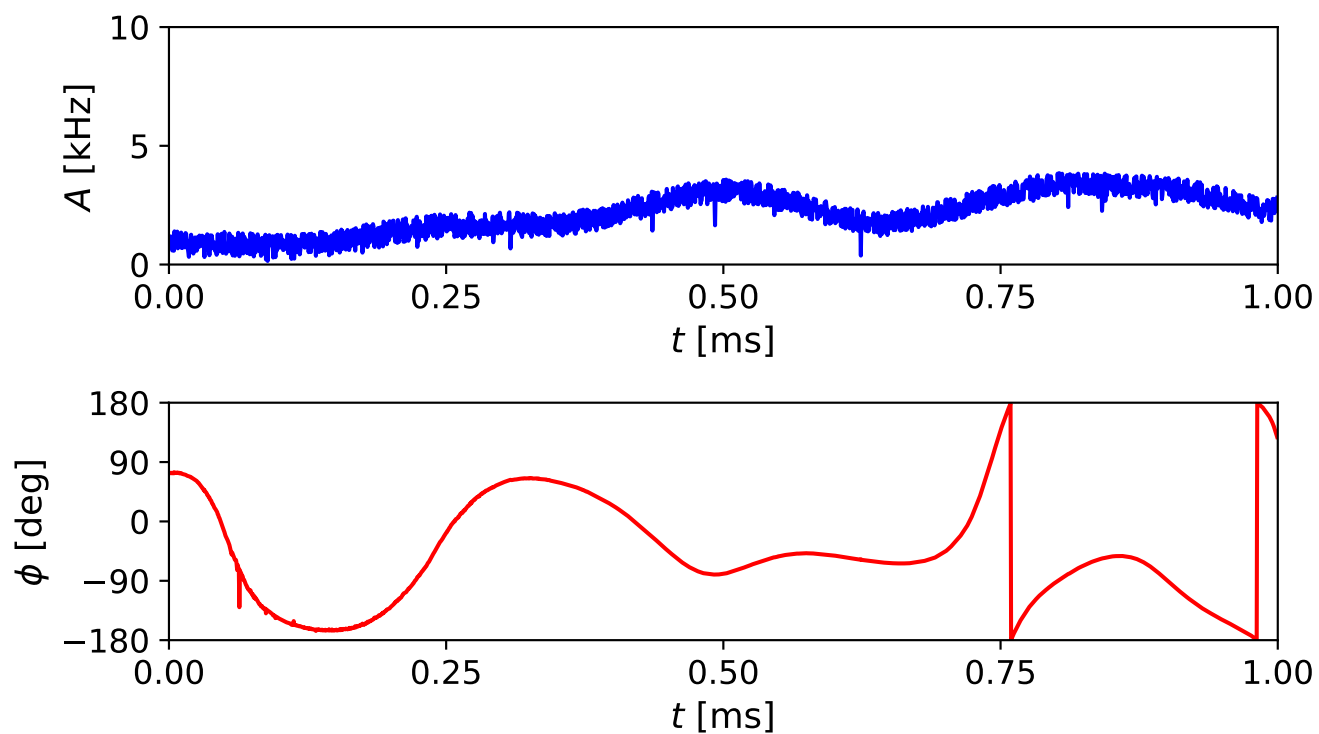


Figure S9. Pulse amplitude A and phase ϕ of nutation-frequency selective excitation for 80 % B_1 increase.

2 Excitation Profiles

35 2.1 Larmor-frequency selective pulses

2.1.1 B_1 -robust selective excitation within ± 500 Hz in a ± 2000 Hz suppression band

Figure S10 shows the excitation profile of the pulse used for B_1 -robust, selective excitation within ± 500 Hz in a ± 2000 Hz suppression band presented in Sec. 3.1 (Fig. 3) of the main article.

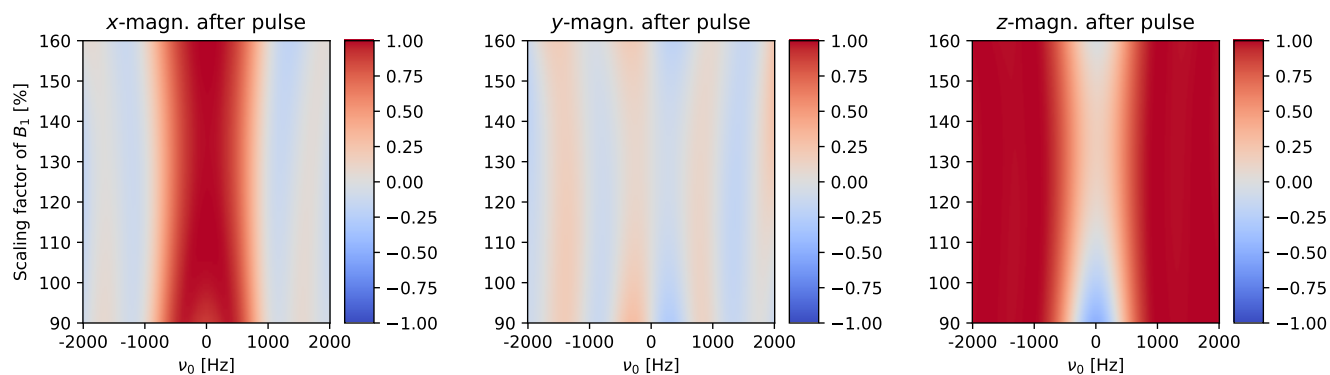


Figure S10. Simulated final x -, y - and z -magnetization for various Larmor-frequency offsets and B_1 increases after applying QOC pulse for Larmor-frequency selective excitation.

2.1.2 B_1 -robust selective suppression within ± 500 Hz in a ± 2000 Hz excitation band

40 Figure S11 and S12 below show the excitation profiles of the pulses used for B_1 -robust, selective suppression within ± 500 Hz in a ± 2000 Hz excitation band presented in Sec. 3.1 of the main article. The experimental results in Sec. 3.1, Fig. 4 were obtained with the pulse in Fig. S12.

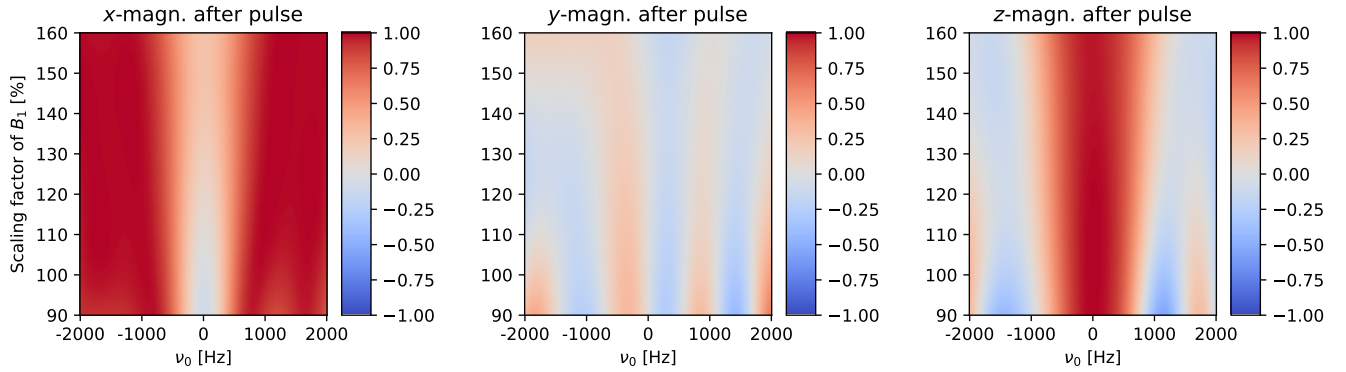


Figure S11. Simulated final x -, y - and z -magnetization for various Larmor-frequency offsets and B_1 increases after applying a 1 ms QOC pulse for Larmor-frequency selective suppression.

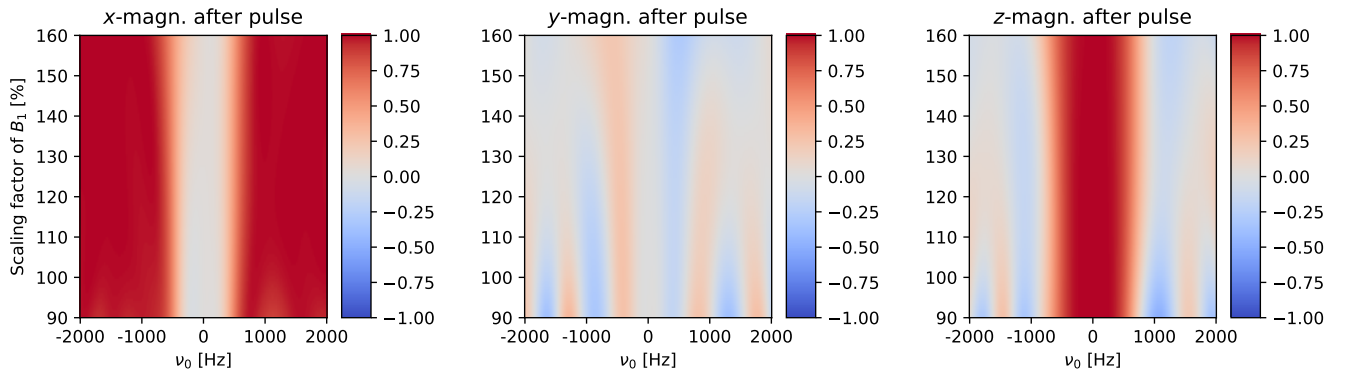


Figure S12. Simulated final x -, y - and z -magnetization for various Larmor-frequency offsets and B_1 increases after applying a 2 ms QOC pulse for Larmor-frequency selective suppression.

2.2 Nutation-frequency selective pulses

The following Figures S13 to S18 show the excitation profiles of the pulses used for Larmor-frequency-robust, selective excitation for various artificial nutation frequency increases presented in Sec. 3.2 (Fig. 6) of the main article.

2.2.1 Larmor frequency-robust selective excitation for 0 % artificial nutation frequency increase

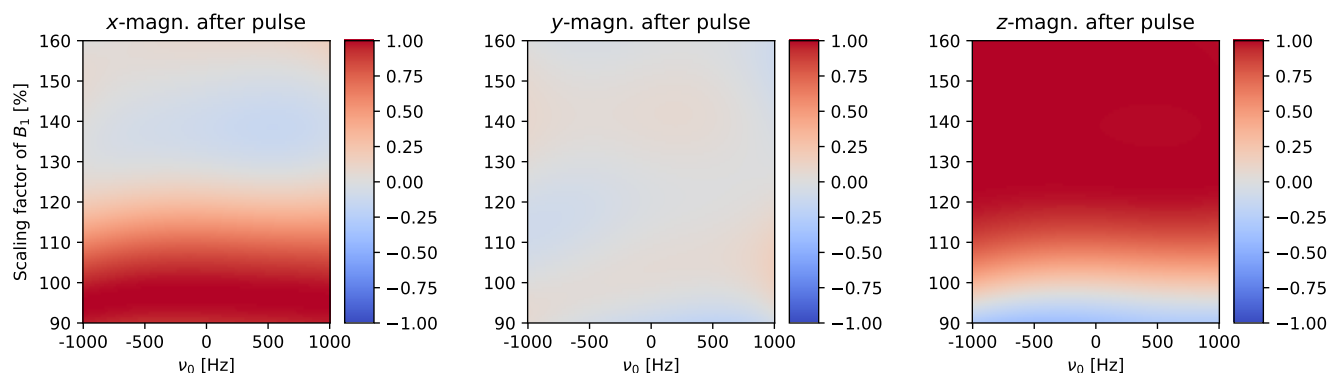


Figure S13. Simulated final x -, y - and z -magnetization for various Larmor-frequency offsets and B_1 increases after applying QOC pulse for nutation-frequency selective excitation for no B_1 increase.

2.2.2 Larmor frequency-robust selective excitation for 20 % artificial nutation frequency increase

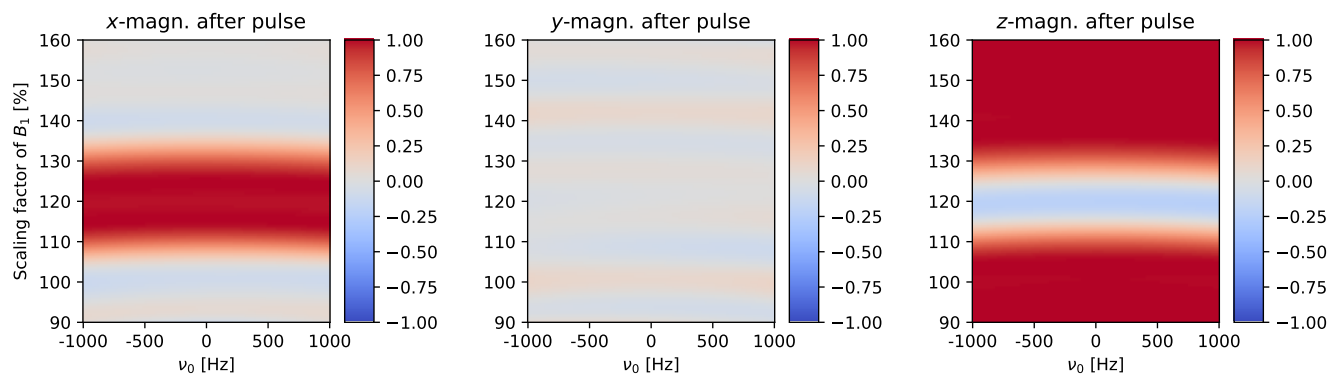


Figure S14. Simulated final x -, y - and z -magnetization for various Larmor-frequency offsets and B_1 increases after applying QOC pulse for nutation-frequency selective excitation for 20 % B_1 increase.

2.2.3 Larmor frequency-robust selective excitation for 25 % artificial nutation frequency increase

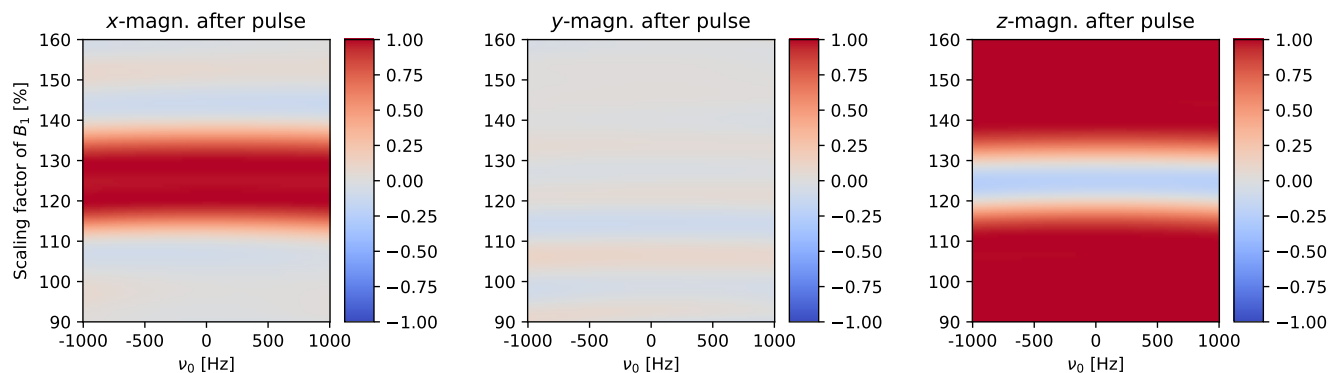


Figure S15. Simulated final x -, y - and z -magnetization for various Larmor-frequency offsets and B_1 increases after applying QOC pulse for nutation-frequency selective excitation for 25 % B_1 increase.

2.2.4 Larmor frequency-robust selective excitation for 30 % artificial nutation frequency increase

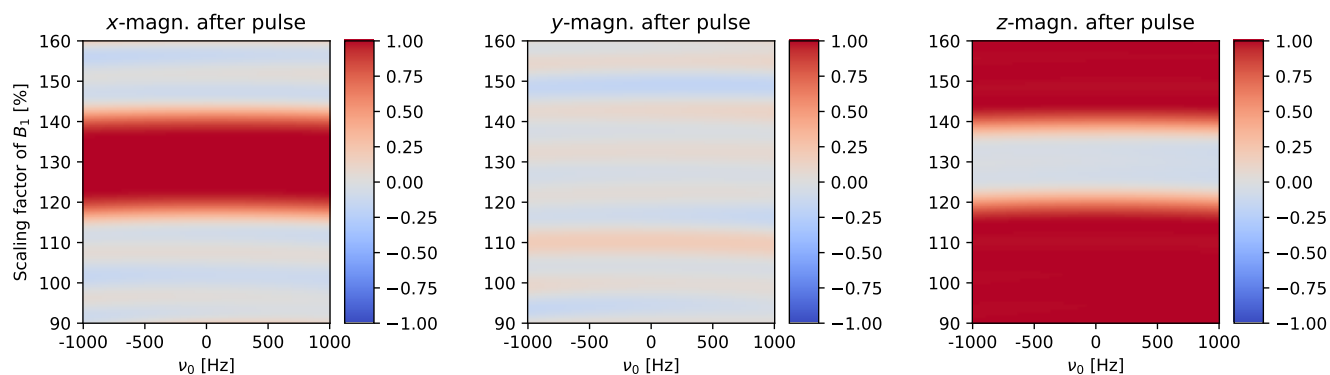


Figure S16. Simulated final x -, y - and z -magnetization for various Larmor-frequency offsets and B_1 increases after applying QOC pulse for nutation-frequency selective excitation for 30 % B_1 increase.

50 2.2.5 Larmor frequency-robust selective excitation for 40 % artificial nutation frequency increase

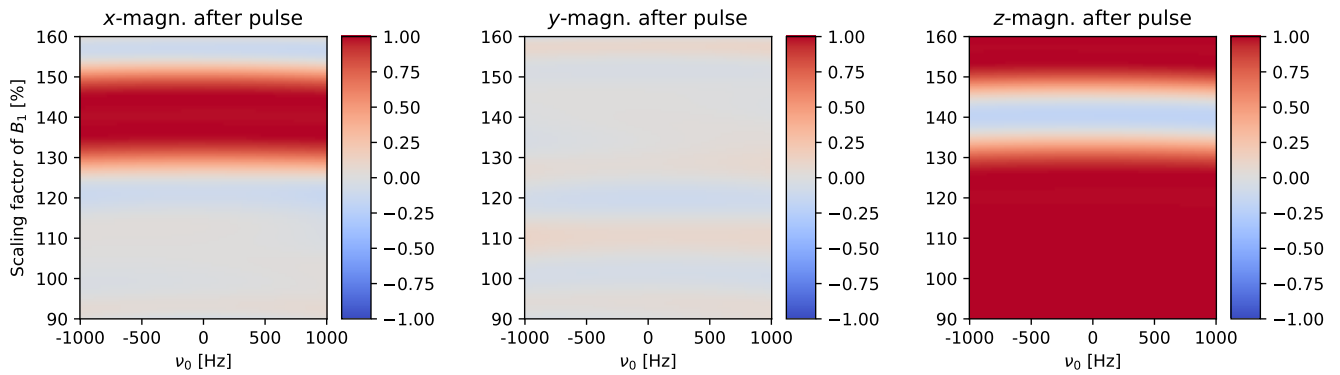


Figure S17. Simulated final x -, y - and z -magnetization for various Larmor-frequency offsets and B_1 increases after applying QOC pulse for nutation-frequency selective excitation for 40 % B_1 increase.

2.2.6 Larmor frequency-robust selective excitation for 80 % artificial nutation frequency increase

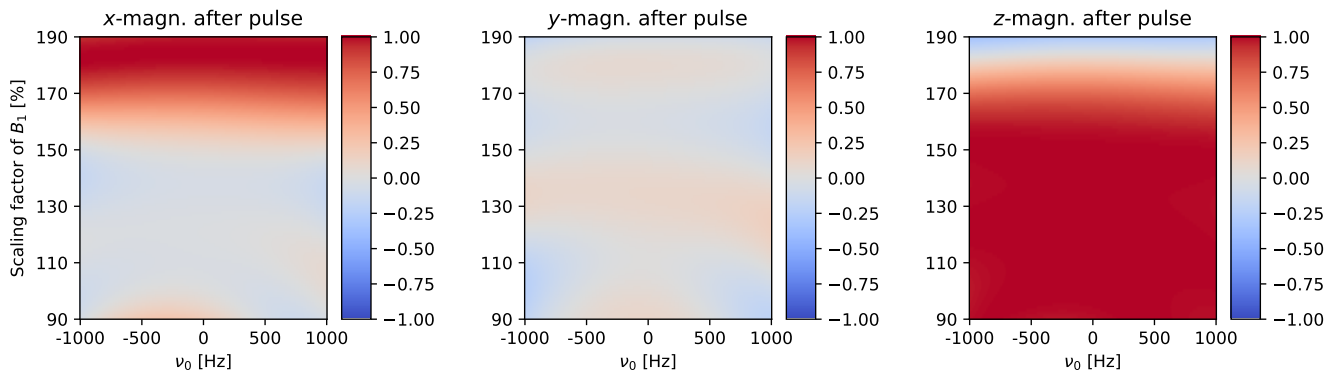


Figure S18. Simulated final x -, y - and z -magnetization for various Larmor-frequency offsets and B_1 increases after applying QOC pulse for nutation-frequency selective excitation for 80 % B_1 increase.

3 Experimental Setup

3.1 Setup in FEM simulation

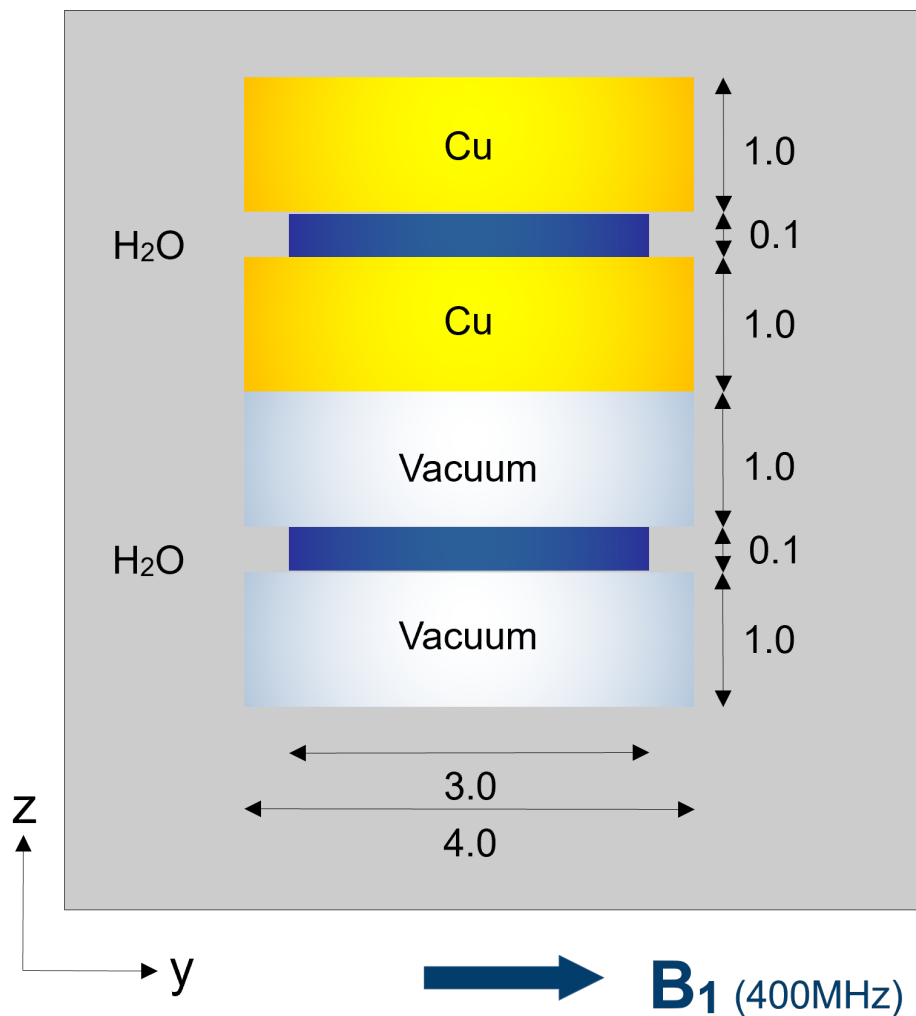


Figure S19. Cell parameters of the model setup in the FEM simulation. The volume between the polymer double coin was introduced as if in-between two cylindrical volumes of vacuum which have a conductivity of zero. Water was adopted as the corresponding liquid in both cavities, as the liquid composition does not affect Γ_{B_1} . The independence was verified by also simulating with *n*-dodecane as corresponding liquid for both cavities or only for the copper cavity.

4 Supporting measurements

55 4.1 Nutation experiments

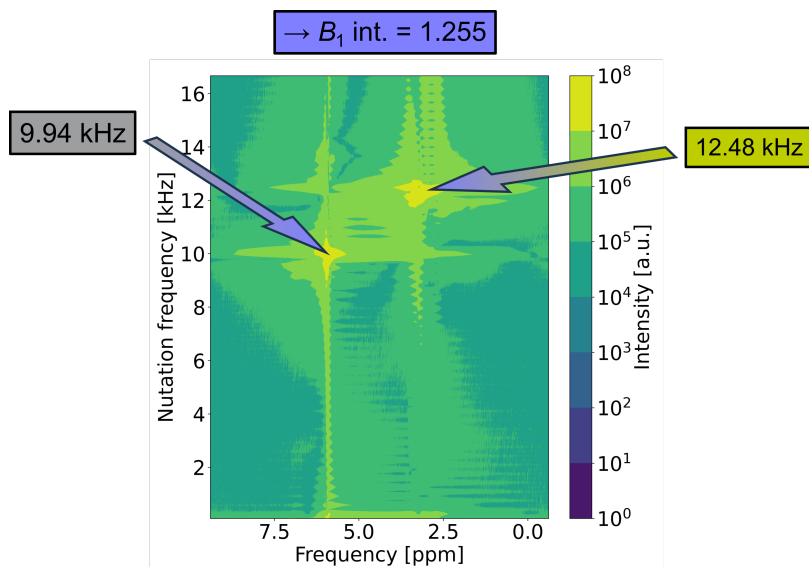


Figure S20. ^1H NMR 2D spectrum of the model setup, describing the intensity distribution of nutation frequencies in dependence of their respective Larmor frequency. The experimentally determined nutation frequency of H_2O is denoted in the grey box while the nutation frequency of *n*-dodecane is denoted in the bright green box. A color gradient from dark blue to bright green is used to illustrate the range from low to high signal intensities.

4.2 B_1 -selective QOC pulse performance

4.2.1 B_1 -selective QOC pulse performance dependence on the liquid composition

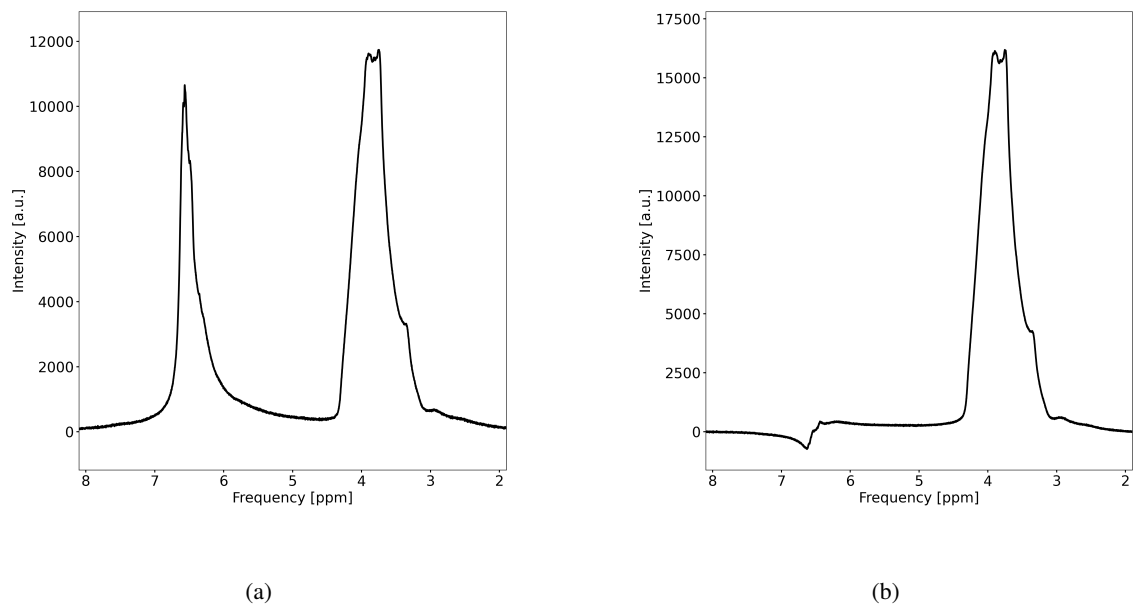


Figure S21. Comparison of the ^1H NMR spectrum of the model setup for a 90° hard pulse (a) to a QOC pulse optimized for $\Gamma_{B_1} = 1.2$ (b). Hereby, the resonance at approx. 3.8 ppm is assigned to *n*-dodecane inside the copper cavity while the signal at approx. 6.5 ppm is assigned to H_2O in the PEEK cavity.

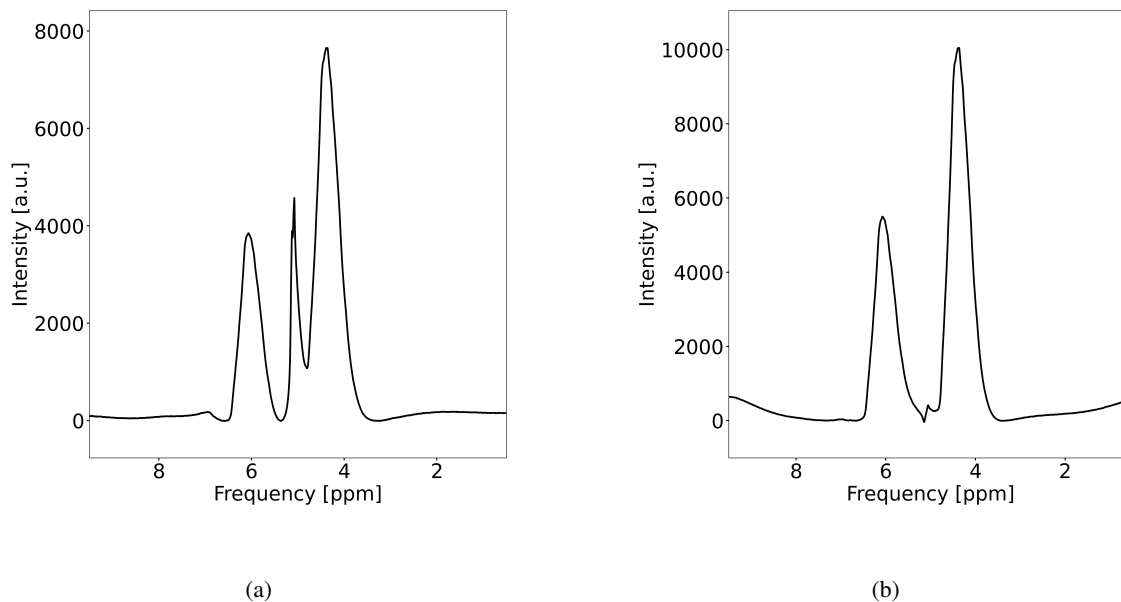


Figure S22. Comparison of the ¹H NMR spectrum of the model setup for a 90° hard pulse (a) to a QOC pulse optimized for $\Gamma_{B_1} = 1.2$ (b). Hereby, the resonances at approx. 4.2 and 6 ppm are assigned to dimethylsulfoxide inside the copper cavity while the signal at approx. 5 ppm is assigned to H₂O in the PEEK cavity. The H₂O resonance is as effectively suppressed as in SI Fig. S21.

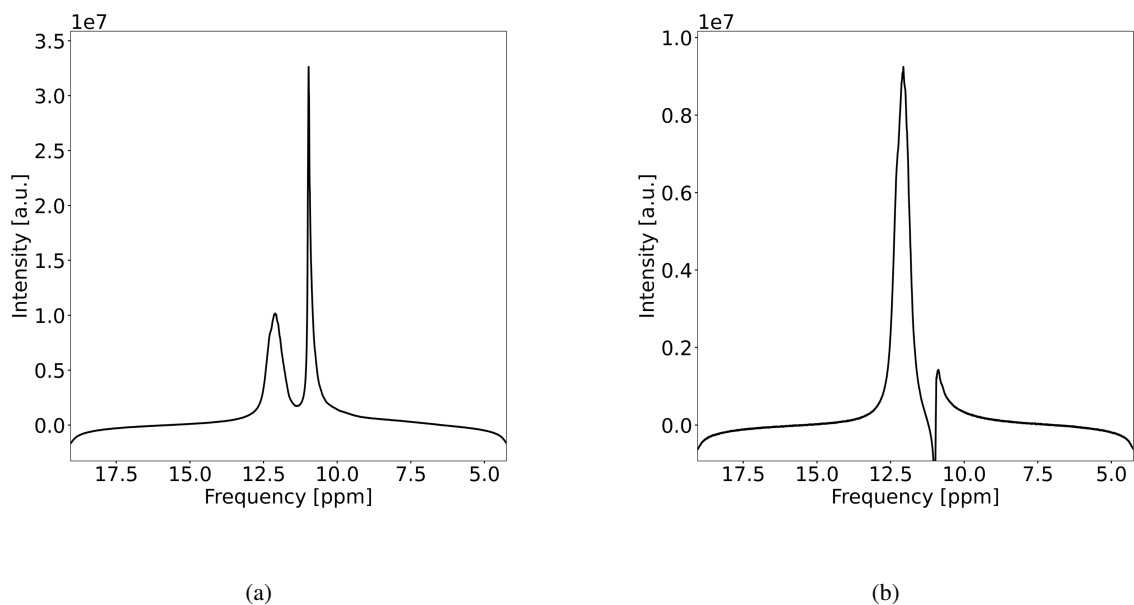


Figure S23. Comparison of the ¹H NMR spectrum of the model setup for a 90° hard pulse (a) to a QOC pulse optimized for $\Gamma_{B_1} = 1.2$ (b). Hereby, the resonance at approx. 10.5 ppm is assigned to H₂O inside the copper cavity while the signal at approx. 12 ppm is assigned to H₂O in the PEEK cavity. The H₂O resonance in-between PEEK is as effectively suppressed as in SI Fig. S21.

4.2.2 B_1 -selective QOC pulse performance dependence on receiver gain

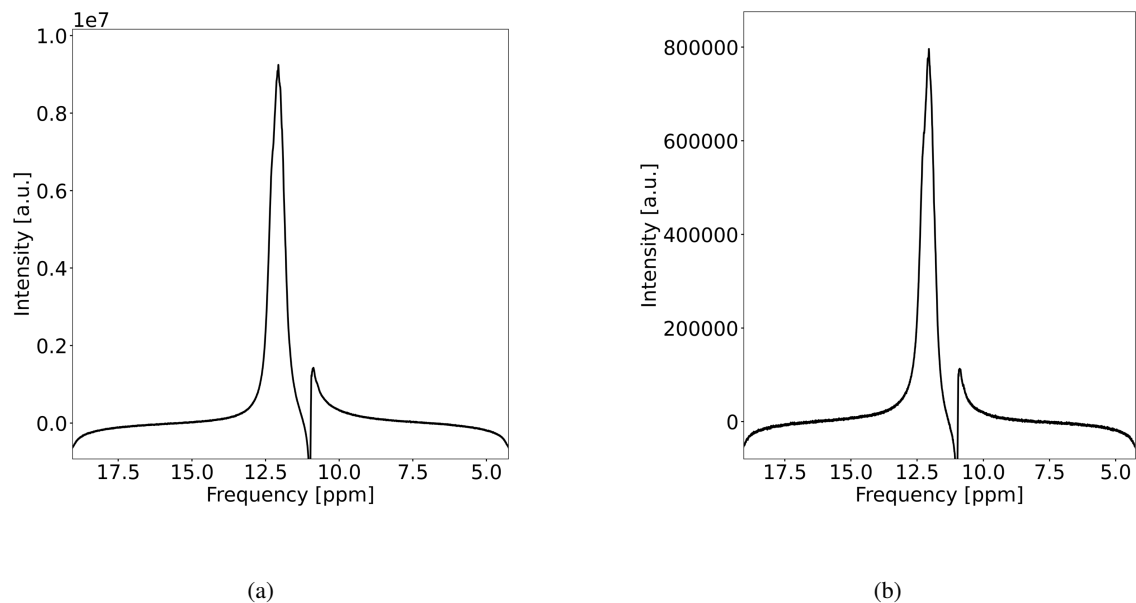


Figure S24. Comparison of the ^1H NMR spectrum of the model setup for a QOC pulse optimized for $\Gamma_{B_1} = 1.2$ with a receiver gain of 1 (a) to a receiver gain of 36 (b). Hereby, the resonance at approx. 10.5 ppm is assigned to H_2O inside the copper cavity while the signal at approx. 12 ppm is assigned to H_2O in the PEEK cavity. The H_2O resonance in-between PEEK is effectively suppressed for both receiver gains.

4.2.3 B_1 -selective QOC pulse performance dependence on shim

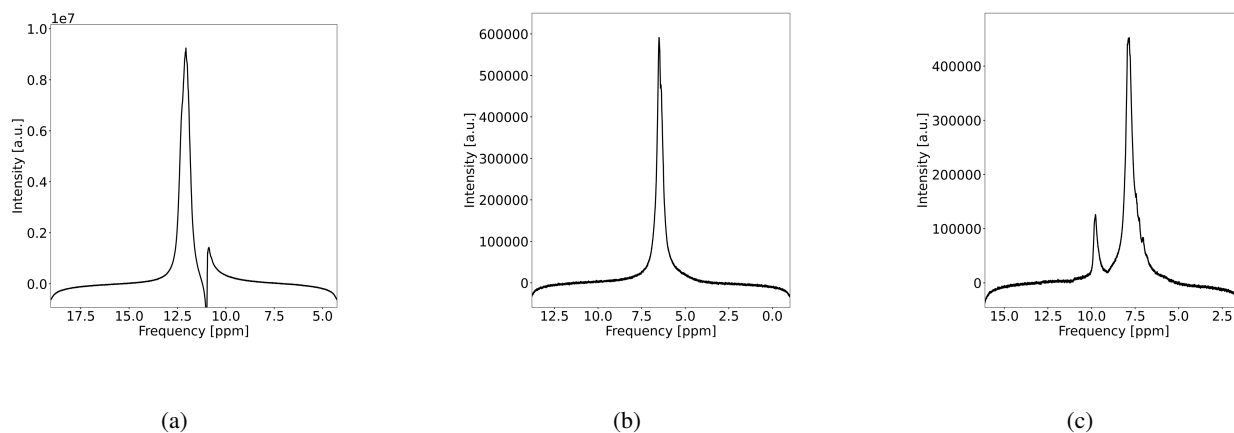


Figure S25. Comparison of the ^1H NMR spectrum of the model setup for a QOC pulse optimized for $\Gamma_{B_1} = 1.2$ with all shims set to zero (a), shimming until both resonances coalesce to a single resonance (b) and shimming to switch the frequencies of both resonances (c). Hereby, the resonance in (a) at approx. 10.5 ppm is assigned to H_2O inside the copper cavity while the signal at approx. 12 ppm is assigned to H_2O in the PEEK cavity. The resonance in (c) at approx. 7.5 ppm is assigned to H_2O inside the copper cavity while the signal at approx. 9.5 ppm is assigned to H_2O in the PEEK cavity. The H_2O resonance in-between PEEK is effectively suppressed in the case of all investigated shims.

60 4.2.4 B_1 -selective QOC pulse performance dependence on $\Delta\nu_0$

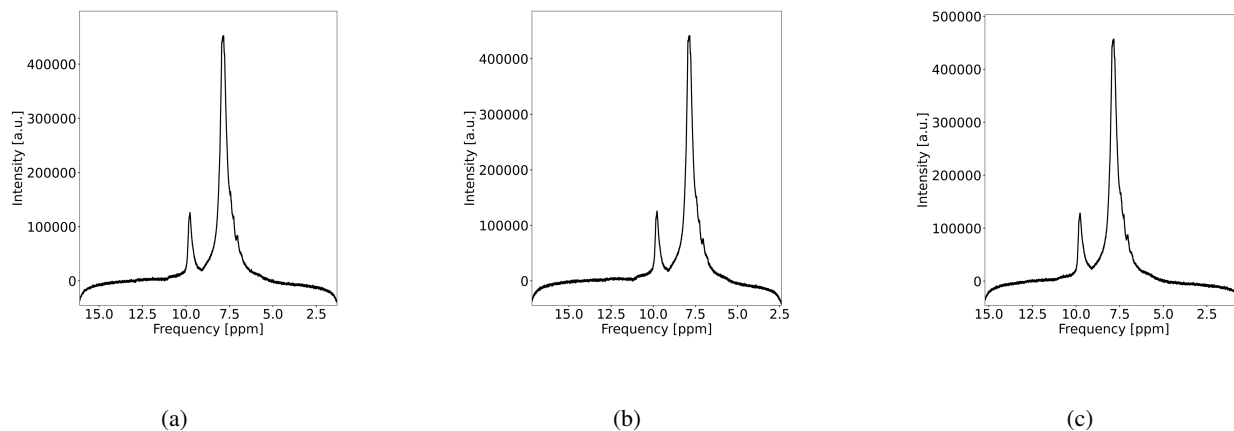


Figure S26. Comparison of the ^1H NMR spectrum of the model setup for a QOC pulse optimized for $\Gamma_{B_1} = 1.2$ with $\Delta\nu_0$ given in Section 2.2 (a), when moving $\Delta\nu_0$ downfield (b) and when moving $\Delta\nu_0$ upfield (c). Hereby, the resonance in (a) at approx. 7.5 ppm is assigned to H_2O inside the copper cavity while the signal at approx. 9.5 ppm is assigned to H_2O in the PEEK cavity. The H_2O resonance in-between PEEK is effectively suppressed in the case of all investigated $\Delta\nu_0$.

4.3 B_0 -selective QOC pulses

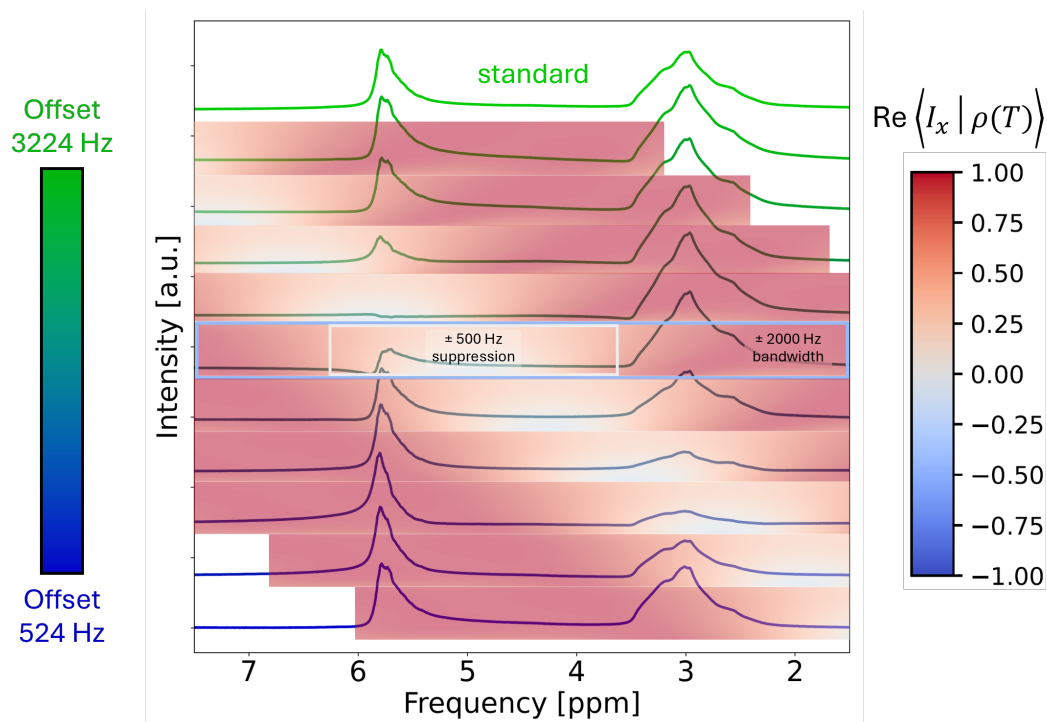


Figure S27. ^1H spectra recorded utilizing a B_0 -selective suppression pulse with a selective suppression range of 2.5 ppm (± 500 Hz), 1 ms duration, and a total frequency range of 4000 Hz applied at different $\Delta\nu_0$. The top spectrum depicts the reference ^1H spectrum recorded using a hard pulse. Hereby, the resonance at approx. 3 ppm is assigned to n -dodecane and the resonance at approx. 6 ppm to H_2O . The spectra recorded with QOC pulses are overlaid with colour gradients representing the theoretical x -magnetization $\text{Re}\langle I_x | \rho(T) \rangle$ after applying the QOC pulse at each particular $\Delta\nu_0$. Selective suppression is achieved for the on-resonance pulse with $\Delta\nu_0 = 2324$ Hz for H_2O . The pulse for n -dodecane is slightly off-resonance (+ 100 Hz) with $\Delta\nu_0 = 1424$ Hz and does not achieve sufficient suppression.

5 Supporting data

5.1 Individual relative integrals of the B_0 -selective QOC pulses

Table S1. Individual relative integrals of the B_0 -selective 1 ms excitation pulses compared to a corresponding 90° hard pulse

| $\Delta\nu_0$ [Hz] | H ₂ O excitation [%] | <i>n</i> -dodecane excitation [%] |
|--------------------|---------------------------------|-----------------------------------|
| 2975 | 66.58 ± 0.41 | 0.90 ± 0.26 |
| 2775 | 95.15 ± 0.38 | 7.56 ± 0.24 |
| 2575 | 87.39 ± 0.36 | 11.56 ± 0.23 |
| 2375 | 87.45 ± 0.43 | 4.96 ± 0.28 |
| 2175 | 97.18 ± 0.38 | 9.71 ± 0.24 |
| 1975 | 95.03 ± 0.36 | 34.30 ± 0.23 |
| 1775 | 70.80 ± 0.37 | 63.17 ± 0.24 |
| 1575 | 35.81 ± 0.40 | 95.45 ± 0.26 |
| 1375 | 4.02 ± 0.40 | 115.34 ± 0.26 |
| 1175 | 13.58 ± 0.40 | 139.11 ± 0.26 |
| 975 | 14.40 ± 0.37 | 77.78 ± 0.24 |
| 775 | 8.89 ± 0.46 | 59.63 ± 0.30 |

Table S2. Individual relative integrals of the B_0 -selective 1 ms suppression pulses compared to a corresponding 90° hard pulse. For this experiment, the baseline of the hard pulse spectrum required a comparatively strong correction, resulting in reduced integrals of the reference spectrum and thus increased relative integrals for all other spectra.

| $\Delta\nu_0$ [Hz] | H ₂ O excitation [%] | <i>n</i> -dodecane excitation [%] |
|--------------------|---------------------------------|-----------------------------------|
| 3224 | 175.34 ± 0.99 | 147.67 ± 0.31 |
| 2924 | 138.48 ± 1.41 | 134.16 ± 0.44 |
| 2624 | 57.89 ± 0.81 | 143.20 ± 0.25 |
| 2324 | 7.42 ± 0.97 | 159.24 ± 0.30 |
| 2024 | 65.17 ± 1.07 | 138.80 ± 0.33 |
| 1724 | 139.83 ± 1.09 | 88.81 ± 0.34 |
| 1424 | 173.06 ± 1.03 | 32.66 ± 0.32 |
| 1124 | 167.19 ± 0.94 | 25.24 ± 0.29 |
| 824 | 168.55 ± 1.11 | 68.70 ± 0.35 |
| 524 | 213.95 ± 0.99 | 110.54 ± 0.31 |

Table S3. Individual relative integrals of the B_0 -selective 2 ms suppression pulses compared to a corresponding 90° hard pulse

| $\Delta\nu_0$ [Hz] | H ₂ O excitation [%] | <i>n</i> -dodecane excitation [%] |
|--------------------|---------------------------------|-----------------------------------|
| 2975 | 86.27 ± 0.46 | 99.92 ± 0.28 |
| 2775 | 40.62 ± 0.43 | 113.72 ± 0.26 |
| 2575 | 5.31 ± 0.41 | 93.40 ± 0.25 |
| 2375 | 1.01 ± 0.48 | 100.00 ± 0.30 |
| 2175 | 5.36 ± 0.45 | 90.79 ± 0.28 |
| 1975 | 34.54 ± 0.36 | 80.60 ± 0.22 |
| 1775 | 81.30 ± 0.43 | 51.14 ± 0.26 |
| 1575 | 102.77 ± 0.40 | 15.44 ± 0.24 |
| 1375 | 111.01 ± 0.42 | 1.29 ± 0.26 |
| 1175 | 119.03 ± 0.53 | 1.14 ± 0.33 |
| 975 | 103.97 ± 0.45 | 19.33 ± 0.28 |
| 775 | 99.13 ± 0.48 | 51.40 ± 0.30 |